Materials Advances

ROYAL SOCIETY OF CHEMISTRY

PAPER

View Article Online
View Journal

Cite this: DOI: 10.1039/d6ma00574h

Synthesis and testing of double-target molecularly imprinted composite polymer (MIP) membranes for selective adsorption of 17β-estradiol and testosterone

Jane Neshovski,[a] Daniel Breite,[a] Zahra Niavarani,[a] Andrea Prager,[a] Dirk Enke[b] and Agnes Schulze*[a]

This study focused on the development and assessment of composite microfiltration (MF) membranes for the selective adsorption-based removal of endocrine-disrupting compounds (EDCs), specifically 17β-estradiol (E2) and testosterone (TST), as emerging hazardous micropollutants in drinking water and natural water sources. The preparation of the composite membranes combined polyethersulfone (PES) with molecularly imprinted polymer (MIP) particles, synthesized through precipitation polymerization. Molecular imprinting was performed by utilizing E2 and TST as templates to create specific recognition sites, while non-imprinted polymers (NIPs) served as references. With the deposition of a MIP/NIP particle layer between two PES layers, sandwich-type composite membranes were prepared and further characterized using scanning electron microscopy (SEM), water permeance, and EDC adsorption tests, which were central to evaluating the effectiveness of molecular imprinting in the MIP-based composite membranes. By comparing EDC adsorption loadings between reference PES and composite membranes through dynamic adsorption experiments, the study assessed the adsorption capacity, selectivity and reusability of the membranes after regeneration cycles. The main objective was to determine whether double-target MIP particles for E2 and TST could be synthesized and incorporated into composite membranes with dual selectivity. Following successful membrane integration, imprinting, and synthesis, the double-target MIP membranes efficiently adsorbed TST (0.48 μg mg^{-1}) and E2 (0.51 μg mg^{-1}). Membrane reusability was tested, revealing that composite membranes do not lose adsorption capacity over at least three cycles. Double-target MIP membranes show promise in effective, low-pressure, low-energy removal of EDCs in water treatment applications.

Received 23rd April 2026,
Accepted 4th June 2026

DOI: 10.1039/d6ma00574h

rsc.li/materials-advances

Introduction

Exposure to various chemical compounds in water, such as endocrine-disrupting chemicals (EDCs) has emerged as a global issue due to their ability to disrupt hormonal function in humans and harm aquatic ecosystems. These micropollutants have been associated with reproductive issues, obesity, and various cancers in humans. One of these EDCs, 17β-estradiol (E2) is the most important natural estrogen hormone, influencing the entire organism and playing a key role in numerous metabolic processes.[1] Moreover, another known EDC is testosterone (TST), which naturally occurs as an androgen steroid hormone, responsible for the development of male reproductive organs and secondary sexual characteristics.[2] Trace concentrations (ng L^{-1} to μg L^{-1}) of EDCs have been detected in both natural and drinking water.[3] Conventional water and wastewater treatment processes are largely ineffective at removing EDCs due to their unique properties and trace concentrations, prompting research into alternative treatment methods.[4,5] Physical treatment techniques, such as membrane filtration and adsorption with adsorber particles are regarded as accessible, fast, and environmentally-friendly methods.[6] Using adsorbents alone leads to saturation over time, requiring replacement or regeneration, which generates hazardous waste and increases costs and maintenance demands.[7,8] Membrane filtration is widely used in advanced water treatment to remove EDCs. Nanofiltration (NF) and reverse osmosis (RO) membranes provide high selectivity, but due to their high-pressure operation, the energy demand increases.[9–11] These systems primarily remove EDCs through adsorption on the membrane surface, based on chemical interactions with the membrane.[12,13] Microfiltration

[a] Leibniz Institute of Surface Engineering (IOM), Permoserstraße 15, 04318 Leipzig, Germany. E-mail: agnes.schulze@iom-leipzig.de
[b] Institute of Chemical Technology, Universität Leipzig, Linnéstraße 3, 04103 Leipzig, Germany

(MF) membranes, such as those made from polyethersulfone (PES), offer a lower-pressure, more cost-effective alternative, while featuring extensive surface area, chemical resistance and high porosity.[14] However, MF membranes alone have demonstrated limited effectiveness in removing EDCs, as their selectivity relies primarily on surface adsorption rather than size exclusion.[15,16] Once the membrane surface becomes saturated, its EDC retention efficiency significantly decreases. Therefore, various adsorption-based water treatment methods, such as activated carbon (AC) and graphene oxide (GO) could be deployed to selectively remove EDCs from water. However, both materials face limitations in sustainability and selectivity.[17] Despite the low cost and availability, AC lacks on-site regeneration methods and typically requires energy-intensive thermal regeneration, leading to higher CO_2 emissions. Additionally, the repeated use of GO reduces its adsorption capacity due to the loss of surface functional groups.[7,18,19] Despite this, adsorber particles remain a promising approach for EDC removal. This includes molecularly imprinted polymer (MIP) particles, which operate based on the principle of molecular imprinting. This process creates selective binding sites for a target analyte within a polymer matrix, which serve as memory sites that specifically recognize and bind to the target molecules.[20] Precipitation polymerization produces spherical MIP particles with well-defined binding sites. In this method, a functional monomer and cross-linker are polymerized in the presence of a template molecule, which initiates the formation of the imprint sites. During polymerization, the monomer interacts with the template to form a stable complex, while the cross-linked polymer backbone keeps the functional groups in specific orientations. After the end of the polymerization, the template is removed, leaving behind cavities that correspond to its size, shape, and spatial orientation (Fig. 1). At the molecular level, the template molecules (E2, TST or both) interact with the functional monomer, such as methacrylic acid (MAA), through hydrogen bonding between its carboxyl group and a hydroxyl group of the template, thus forming a stable complex, fixed within the cross-linked polymer matrix.[21,22] The rigid hydrocarbon structure of the templates limits their possible spatial orientations, promoting the formation of well-defined recognition sites.[23] As illustrated in Fig. 1, the binding pockets are formed around individual template molecules, allowing accommodation of one target molecule at a time. Although multiple functional groups within a pocket allow for multipoint interactions, simultaneous binding of more than one molecule per site is unlikely.[24] In addition to hydrogen bonding, hydrophobic and π–π interactions further contribute to the overall binding of the molecules within the binding pocket.[25–27] When both templates are used, a wider variety of binding site geometries is formed, enabling recognition of structurally related hormones and extending the use of single-template MIP system to a wider class of EDCs.[28]

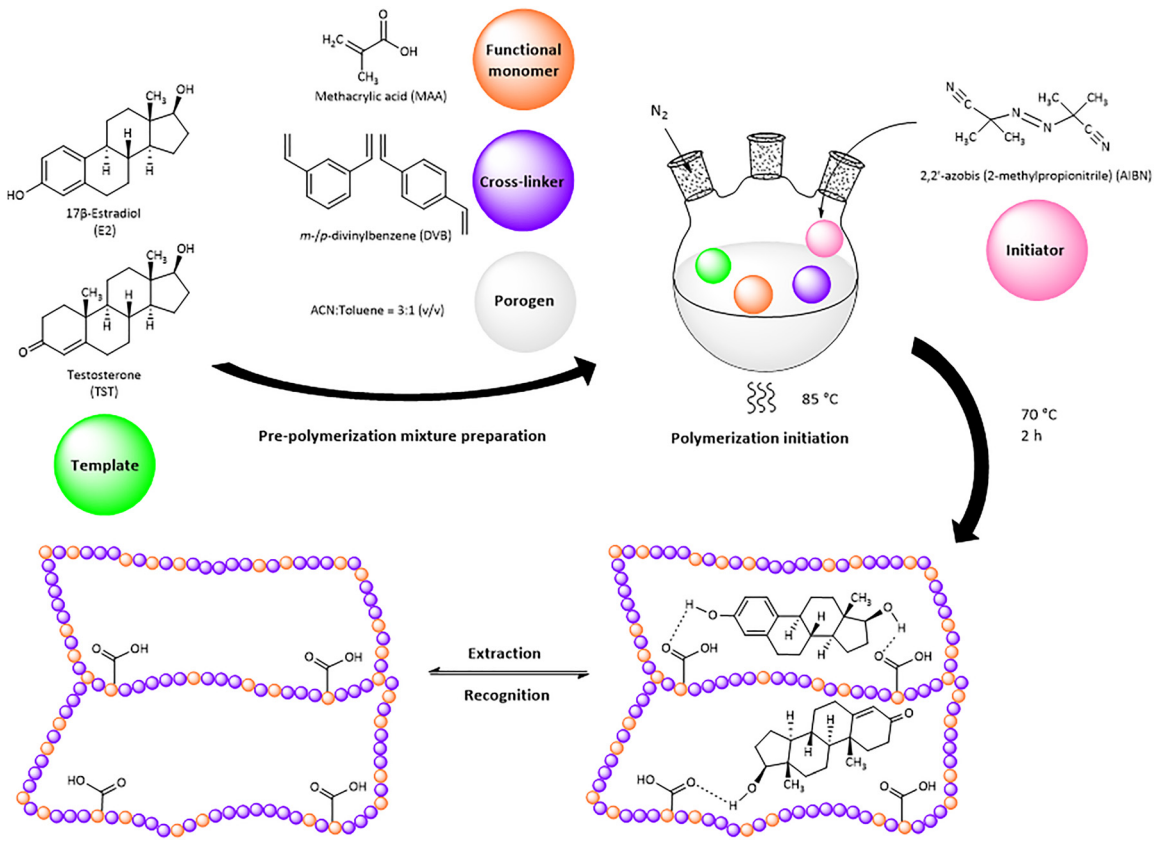

Fig. 1 Scheme of precipitation polymerization and template (E2 and TST) molecular imprinting process.

The formed cavities exhibit high affinity and selectivity toward the target molecule.[29–38] Non-imprinted polymers (NIPs) share the same chemical composition as MIPs but are synthesized without the template, resulting in the absence of specific recognition sites. Therefore, MIPs demonstrate stronger binding interactions with target molecules than NIPs, with the effectiveness of these interactions depending on how well defined the cavities are, which can be assessed through their adsorption capacity.[39] Previous studies have reported the synthesis of MIPs through precipitation polymerization.[40,41] In these studies, MAA was used as the functional monomer, while divinylbenzene (DVB), trimethylolpropane trimethacrylate (TRIM), or ethylene glycol dimethacrylate (EGDMA) served as cross-linkers. Molecular imprinting was performed in the presence of an EDC acting as the template molecule, resulting in MIP-EDC particles specifically tailored for EDC recognition. When E2 was used as the template, the resulting MIPs were E2-imprinted particles.[41] The adsorption capacity and selectivity of MIPs have been extensively investigated, mainly by exploring different polymerization methods and different monomer units. As previously mentioned, precipitation polymerization was utilized to prepare MIPs designed to specifically recognize E2.[40] The polarity of the solvent during polymerization further played a crucial role in determining the adsorption capacity of the MIPs for E2, as evidenced by the use of acetonitrile as the porogen.[42] Furthermore, 100 mg of MIP microspheres prepared using 4-vinylpyridine and TRIM as the functional monomer and cross-linker, respectively, exhibited high selectivity and efficiency, removing more E2 than 300 mg of AC. Notably, these MIPs demonstrated excellent reusability, maintaining their performance for up to 30 cycles.[43]

As previously described, MF membranes alone exhibit certain limitations in selectivity towards EDCs, which could be improved by certain modification or integration of other materials to achieve higher EDC removal. Incorporating adsorber particles into the matrix of these membranes results in obtaining composite membranes.[41,44] Materials such as AC, zeolites, or clays could serve as these adsorbents, whose incorporation in the membrane significantly improves membrane performance, yielding adsorption capacities between 80% and 90% for various EDCs, due to the effective adsorption through multiple interaction mechanisms.[45,46] Furthermore, composite membranes produce less waste since the incorporated adsorber particles can be easily regenerated and reused, making them sustainable without the need for frequent replacement.[41] Several studies have focused on the development of composite membranes to enhance their efficiency in micropollutant adsorption. To remove pharmaceuticals from water, one study focused on synthesizing mixed matrix membrane adsorbers that incorporated three different types of anion exchange particles. Some of the investigated pharmaceuticals, like diclofenac and sulfamethoxazole, were reported to be adsorbed up to 13.7 g m^{-2} and 0.60 g m^{-2}, respectively, onto the adsorbers.[47] Similarly, PES membranes embedded with nanocomposite adsorbers exhibited the ability to remove bisphenol A (BPA) up to 1.2 mg m^{-2}.[48] A further example of incorporating adsorptive particles into MF membranes is the integration of ZnO nanoparticles into PES membranes, which effectively enhanced the adsorption of dyes such as methylene blue rose from 47.5% to 82.3% in the ZnO–PES composite membranes.[49]

An approach in a previous study included the preparation of sandwich-type composite membranes, in which MIPs were trapped between two MF membranes. The MIPs were prepared using MAA as the functional monomer and EGDMA as the cross-linker, with a chiral amino acid derivative serving as the template molecule for imprinting. NIP particles were also synthesized without the template. The composite membranes were then fabricated by depositing the MIP particles as a layer between two MF polyamide membranes, which functioned as the support and cover layers. The selectivity of the resulting composite membranes was confirmed by filtering a racemic mixture containing equal amounts of both enantiomers of the chiral amino acid, where the membrane selectively retained only one enantiomer.[50] This concept could similarly be adapted for the selective removal of EDCs by using not only one EDC molecule, but two EDCs simultaneously as the template in the imprinting process, in order to obtain double-target MIP particles. Composite membranes were then fabricated using these particles, along with NIPs, following the procedure described above. The integration of MIPs into MF membranes aimed to demonstrate that these composite membranes could serve as a promising option for the selective removal of EDCs under low-pressure and low-energy conditions in water treatment applications. Therefore, their performance was evaluated through adsorption experiments.

Experimental

Materials and methods

17β-Estradiol (E2), testosterone (TST), methacrylic acid (MAA), 2,2′-azobis (2-methylpropionitrile) (AIBN), divinylbenzene (DVB), acetic acid, acetonitrile (ACN) and methanol (MeOH) were purchased from Sigma Aldrich (St. Louis, MO, USA). Bisphenol A (BPA) was obtained from Thermo Fisher Scientific (Geel, Belgium). Microporous polyethersulfone (PES) (0.45 μm, Express Plus, Merck Millipore) membranes were purchased from Merck (Darmstadt, Germany). Absolute ethanol (EtOH), toluene and aluminum oxide (Brockmann I) were purchased from VWR (Radnor, PA, USA). Ultra-pure water was generated by using Milli-Q purification system. All materials were used as they were received from suppliers.

Synthesis of MIP/NIP particles

Pre-polymerization mixture preparation. First, the template (1 mmol of E2, TST, or a 1 : 1 mixture of E2 and TST) is dissolved into MAA (8 mmol) and DVB (40 mmol) to create the template solution for each MIP type (E2, TST and the E2-TST mixture). Meanwhile, the molar ratio of 1 : 8 : 40 is kept constant. Without the addition of the template molecule, the ratio of 8 : 40 is maintained while preparing the NIP particles. Equal amounts of both templates are included in 1 mmol of the E2-TST

mixture, while maintaining a consistent ratio of MAA to DVB. In a round-bottom, three-neck flask, 1 mmol of the template was added, followed by 0.7 mL of MAA and 5.7 mL of DVB, pre-filtered through aluminum oxide. The mixture was dissolved in ACN and toluene (3 : 1 v/v) and sonicated for 15 minutes to ensure homogeneity, followed by degassing with nitrogen flow for 20 minutes to remove any dissolved oxygen.

Polymerization initiation and purification. After being sealed in a nitrogen atmosphere, the flask was put in an 85 °C silicon oil bath. 13.77 mg of AIBN or 2 wt% of the monomer weight, were dissolved in ACN and injected through a septum stopper into the flask and continuously stirred at about 180 rpm. The heat was reduced to 70 °C for two hours to finish the polymerization. After the particles settled, they were cleaned with EtOH to get rid of any unreacted compounds. A thorough washing was carried out on the precipitated polymer using a 9 : 1 v/v solution of MeOH and acetic acid. A dozen Eppendorf vials were filled with the mixture, sonicated for 2–3 min, and centrifuged using a micro-centrifuge (Carl Roth, Karlsruhe, Germany). 100 μL of the supernatant solution was gathered and put into a 384-well plate (UV-Star Plate, Greiner Bio-One, Frickenhause, Germany) to determine the quantity of the template molecules through UV absorption or fluorescence detection (Infinite M200, Tecan, Germany). The washing process was carried out eight to ten times until the template molecules could no longer be detected.

Composite membranes

Preparation of sandwich-type composite membranes. The composite membranes were fabricated by cutting dry sheets of microporous PES membranes with 0.45 μm pore size into 47 mm diameter. The sandwich-type composite membrane is supported and covered by a PES membrane, respectively. As a support membrane, a single 47 mm PES membrane disk was placed in the filter holder of a bench scale stainless-steel dead-end filtration device (16 249, Sartorius Stedim Biotech, Göttingen, Germany). The cell was filled with 25 mL of particle suspension containing 0.1 g MIP or NIP in water/EtOH solution (9 : 1 v/v). By adding nitrogen gas at maintained pressure of 30 mbar, the suspension was filtered through the support membrane and particles were deposited onto the membrane's surface. A second 47 mm PES membrane disk was then used to cover the particle layer, resulting in the MIP or NIP sandwich-type membrane.

The synthesized MIP/NIP particles and composite membranes were characterized using a variety of methods, including water permeance, scanning electron microscope (SEM) and EDC adsorption tests. The water permeation experiments were performed on the reference PES membranes and sandwich-type composite membranes to determine their water permeability using a filtration cell, equivalent to the one used to create composite membranes. Two 47 mm PES membrane disks were put in the filter holder of the filtration cell and 100 mL of purified water was added to the cell. 1 bar of nitrogen pressure was applied, and the filtration time was recorded. Similarly, to measure the water permeance of the sandwich-type composite membranes, one 47 mm PES membrane disk was placed in the filter holder. 25 mL of a 0.1 g MIP/NIP particle suspension in water/EtOH solution (9 : 1 v/v) was introduced to the cell. The deposited layer of particles on the support membrane was covered with a second 47 mm PES membrane disk. The filtration time of 100 mL of purified water under 1 bar of nitrogen pressure was measured.

The reference PES and composite membranes' permeation times were measured, with the water permeance J (L m^{-2} h^{-1} bar^{-1}) being calculated based on the outcomes of the filtration tests using eqn (1):

$$J = \frac{V}{t \cdot A \cdot p} \quad (1)$$

where V (L) indicates the volume of filtered water, A (m^2) is the membrane's active surface area, t (h) is the permeation time, and p (bar) is the applied pressure throughout the filtering process.

With the utilization of SEM (Ultra 55, Carl Zeiss Microscopy GmbH, Oberkochen, Germany), the particles' morphology and size was investigated. A silicon wafer was coated with a suspension of MIP/NIP particles in absolute EtOH and left to dry at room temperature. The samples were coated with a thin (30 nm) coating of chromium using the Z400 sputtering system (Leybold, Hanau, Germany). The magnification ranged from 1000 to 25 000 fold. Moreover, the sandwich membrane cross-section was observed using an optical microscope (Olympus DSX1000, Olympus Corporation, Japan) to visualize the composite structure.

Adsorption of EDCs on composite membranes

To examine the adsorption of EDCs on the reference and composite membranes, multiple dynamic adsorption tests were conducted. A stock solution of E2 with a concentration of 10 mg mL^{-1} was prepared by dissolving 100 mg of E2 in 10 mL of absolute EtOH. To prepare a solution with final concentration of 5 mg L^{-1} (5 ppm), 50 μL of the stock E2 solution was added to a 100 mL volumetric flask and diluted with water/EtOH solution (9 : 1 v/v). To create a calibration curve, four more solutions with concentrations of 4, 3, 2, and 1 mg L^{-1} were prepared. The concentrations of the five aqueous E2 solutions were measured through fluorescence detection at an excitation wavelength of 273 nm and an emission wavelength of 305 nm. Similarly, the TST and BPA stock solutions were prepared with a concentration of 10 mg mL^{-1} and subsequently five aqueous TST and BPA solutions (concentrations of 4, 3, 2, and 1 mg L^{-1}) were used to create calibration curves. In the case of the TST solutions, the UV absorbance was measured at a wavelength of 246 nm, whereas the concentration of the BPA solutions was determined by fluorescence detection at an excitation wavelength of 276 nm and emission wavelength of 306 nm. 50 μL of each stock solution of E2 and TST (10 mg mL^{-1}) were sampled into a 200 mL volumetric flask to create the 1 : 1 E2-TST mixed solution. To obtain this solution with a final concentration of 5 mg L^{-1} EDCs (2.5 mg L^{-1} for each EDC), it was diluted to 200 mL with water/EtOH solution (9 : 1 v/v). Table 1

Table 1 Structures of investigated EDC molecules and some properties

MIP/NIP particle and membrane characterization compound	Chemical structure	Molecular weight/g mol^{-1}	TPSA/Å^{2} [51]
17β-Estradiol (E2)	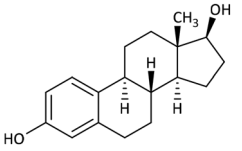	272.4	40.5
Testosterone (TST)	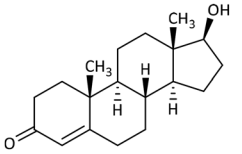	288.4	37.3
Bisphenol A (BPA)	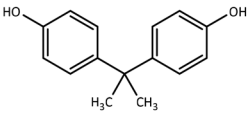	228.3	40.5

lists the EDC molecules studied along with their relevant properties.

To assess the dynamic adsorption loadings of the reference PES and composite membranes, the EDCs aqueous solutions were filtered using filtration equipment as described for the fabrication of the sandwich-type composite membranes. Following the preparation of the composite membrane in the filter holder as detailed in the preceding section, the filtration procedure started by adding 30 mL of water/EtOH solution (1 : 1 v/v) to the membranes under nitrogen pressure of 30 mbar. Afterwards, another 25 mL of a water/EtOH solution (9 : 1 v/v) were filtered. Finally, the adsorption test was conducted by adding 50 mL of 5 mg L^{-1} EDC solution to the membrane system in the filtration cell. Samples were initially collected at 2 mL, 5 mL, and subsequently every 10 mL. The concentrations of each permeate sample were determined by UV absorption or fluorescence detection. This dynamic adsorption experiment approach was performed for a second and third adsorption cycle to test the reusability of the composite membranes. The membranes were thoroughly washed by rinsing them with 30 mL of water/EtOH solution (1 : 1 v/v) following each adsorption cycle. The washing stage involves further adding and filtering 25 mL of water/EtOH solution (9 : 1 v/v) to the filtration apparatus before the next cycle.

50 mL of 5 mg L^{-1} EDC solution was applied to the regenerated composite membranes for a second adsorption cycle, and permeate samples were obtained as in the first cycle. Fluorescence detection or UV absorption were used to measure 100 μL of each permeate sample. With this approach, the membranes' reusability was evaluated, and a third adsorption cycle was carried out using the same process. In the same manner as the sandwich-type composite membranes, the dynamic adsorption and reusability tests were conducted for reference PES membranes using two 47 mm PES membranes without MIP/NIP particles present.

The composite membranes containing particles imprinted with E2 were designated as PES + MIP-E2, while those containing TST-imprinted particles were referred to as PES + MIP-TST. Moreover, the composite membranes that have double-target imprinted particles incorporated, were denoted as PES + MIP-E2-TST. While PES + MIP-E2 and PES + MIP-TST composite membranes were treated with E2, TST and BPA, dynamic adsorption tests were conducted using the same protocol for reference PES and PES + NIP composite membranes with E2, TST, BPA and E2-TST mixture. The E2-TST mixture was used to treat the PES + MIP-E2-TST double-target composite membrane.

Results and discussion

The preparation of MIP/NIP adsorber particles and sandwich-type composite membranes, followed by their characterization and adsorption testing are described and discussed in this section. The preparation process of the particles included precipitation polymerization, and molecular imprinting was employed to obtain the MIPs. A layer of particles was introduced between two MF membranes, thus forming the composite membranes. Water permeance measurements, SEM, and EDC adsorption tests were among the characterization methods used to determine the success of particle synthesis and the composite membrane preparation. As supplementary characterization, optical microscopy of the sandwich membranes showed a cross-section with the particle layer sandwiched between two PES membranes (Fig. S6). Due to wet conditions and the non-adhesiveness of the particles to the surface of the membranes, some particle displacement occurred onto the membrane surface during preparation. Further measurements would require removing the membrane system from the filtration cell, thus altering the structure of the system.

Water permeance

To evaluate the water permeance of the membranes, the reference PES and composite membranes' permeation times were recorded, and water permeance J was calculated using eqn (1). The permeance values for the tested membranes are shown in Fig. 2. The water permeance for the reference PES membranes was measured by stacking two PES membranes on top of one another. They showed an average permeance value of 15 401 ± 298 L m^{-2} h^{-1} bar^{-1}, due to being hydrophilic. Between the support and cover PES membrane, a layer of NIP particles was added to prepare sandwich-type composite membranes. Compared to the reference PES membranes, this led to a significantly reduced water permeance. The composite membranes exhibited an average permeance value of 1243 ± 246 L m^{-2} h^{-1} bar^{-1}, which corresponds to about 8% of the reference PES membranes. Only NIP particles were used for the water permeance studies, as previous work has shown that molecular imprinting does not affect the permeability of composite MIP membranes, as these membranes with embedded MIP particles exhibited consistently good permeability.[41] This is further supported by SEM images of NIP and MIP particles, which show no visual difference (Fig. S2 and S3 in SI), indicating similar filtration behavior, leading to

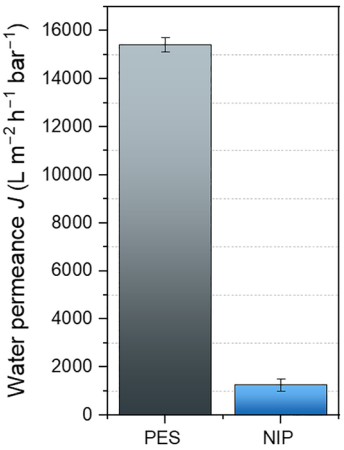

Fig. 2 Water permeance of reference PES and sandwich-type composite membranes.

comparable water permeance for both systems. Due to the additional resistance of the inserted particle layer between the membranes and the trapped air pockets, the noticeable decrease in water permeability of the sandwich-type composite membranes was anticipated. Nonetheless, the addition of MIP/NIP particles to MF membranes, neither caused membrane blockage nor increased the water permeability of the membrane system.

SEM

To analyze the morphology of the adsorber particles as well as the pore structure and morphology of the reference PES membranes, SEM was utilized. The top side (Fig. 3a) and cross-section (Fig. 3b) of the reference PES membrane are shown in Fig. 3. Additionally, Fig. 3c–f shows the structural properties of the adsorber particles. The particles show noticeable spherical forms and the scale on Fig. 3 indicates that their sizes predominantly range from 1 to 2 μm. This demonstrates that the MIP/NIP particles are homogenous in size and shape, in line with earlier studies.[41,52] The small degree of particle agglomeration necessitated the creation of sandwich-type composite membranes, despite the spherical characteristics of the adsorber particles were thought to be appropriate for integration into the membrane scaffold.

Adsorption of EDCs

With the use of 5 mg mL^{-1} aqueous solutions of EDC, a series of dynamic adsorption experiments were conducted to investigate the adsorption characteristics of the reference PES and composite membranes. To evaluate how efficiently and selectively the tested membranes removed E2, TST, BPA, and E2-TST mixture over the course of three cycles, adsorption loadings for the EDCs were calculated. The adsorption cycles were repeated, to determine whether the membranes could be reused. Adsorption loadings for reference PES were determined as a ratio between the quantity of adsorbed EDC on the membranes and the weight of the membranes in total (μg of adsorbed EDC/153.13 mg of PES). Additionally, the ratio between the quantity of adsorbed EDC and the weight of the two PES membranes

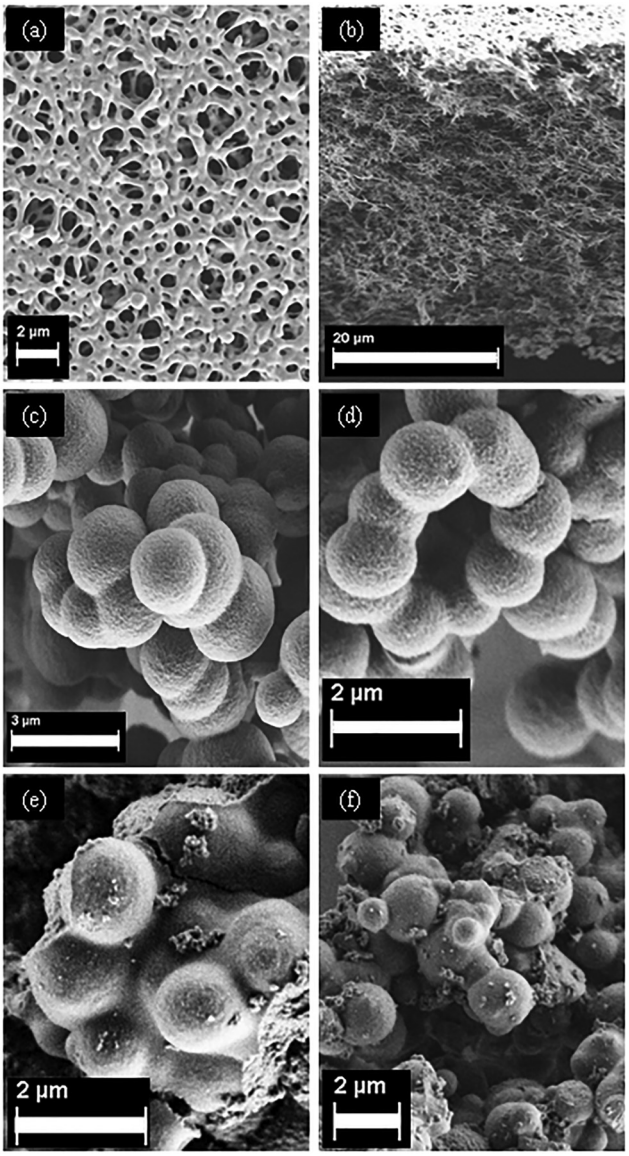

Fig. 3 SEM images of the (a) top side and (b) cross-section of reference PES membrane and (c) NIP, (d) MIP-E2, (e) MIP-TST and (f) MIP-E2-TST adsorber particles.

with an added 100 mg layer of adsorber particles (μg of adsorbed EDC/253.13 mg of PES + MIP/NIP) is used to display the EDCs' adsorption loadings for the composite membranes. For each membrane system, 50 mL of EDC solution was filtered three times with a thorough washing step implemented between each filtration. For every cycle, breakthrough (BT) curves were obtained, providing information on the membranes' adsorption performance. The BT point is defined as the stage in a membrane filtration process when the permeate concentration (Cp) reaches 10% of the feed concentration (C_0).[41] The average values for the adsorption loading were obtained by repeating each dynamic adsorption experiment three times in three cycles.

E2 adsorption loading. Fig. 4 displays the findings for the E2 adsorption loadings over three adsorption cycles for three

membrane systems: PES, PES + NIP, and PES + MIP. After 50 mL of 5 mg L^{-1} E2 solution were filtered through the reference membrane system, consisting of two PES membranes, the average amount of E2 adsorbed was 0.58 ± 0.18 μg mg^{-1} for the first cycle, which was measured three times for each membrane system (Fig. 4). Following the washing step in between each cycle, the E2 adsorption loading for the second and third cycles was further calculated. In the case of the PES + NIP composite membrane, by introducing NIP particles, the E2 adsorption moderately increases, as evident from the E2 adsorption loading of 0.64 ± 0.14 μg mg^{-1} in the first cycle. As the available surface area is greater in the PES + NIP composite membrane than the reference PES membranes, the adsorption loading for the subsequent cycles shows a comparable slight rise. The average adsorption loading for the first cycle for PES + MIP-E2 composite membrane was calculated, yielding a value of 0.62 ± 0.29 μg mg^{-1}. Consecutively, E2 adsorption loading was measured in the second and third cycles, which are 0.80 ± 0.13 μg mg^{-1} and 0.82 ± 0.12 μg mg^{-1}, respectively. Since the values fall mostly within the error bars observed for the previous two membrane systems, PES + MIP-E2 composite membrane shows a slightly gradual increase in the E2 adsorption in the later cycles, indicating a potential modest improvement for further cycles.

Over the three adsorption cycles, BT curves for the tested E2 are composed as shown on Fig. 5. During the span of one filtration cycle, the E2 concentration (mg L^{-1}) in the permeate progressively rises. The reference PES membrane systems achieve a saturation plateau in the second half of each cycle, limiting additional E2 adsorption. In comparison, the E2 concentration in each cycle of the dynamic adsorption experiments with composite membranes can be considered lower than the reference PES. As evidenced by its low presence in the permeate at the start of the subsequent cycle, the adsorbed E2 is washed off with the regeneration phase, implemented after the filtration of 50 mL E2 solution. With the inclination of BT curves for PES + NIP composite membranes, an additional

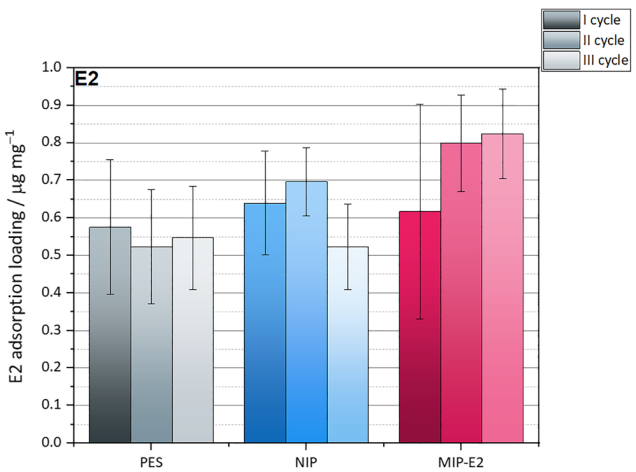

Fig. 4 E2 adsorption loading (μg mg^{-1}) on reference PES, PES + NIP and PES + MIP-E2 in three adsorption cycles.

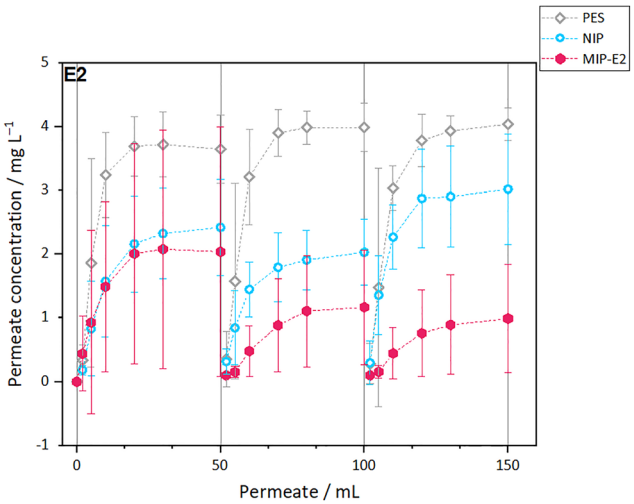

Fig. 5 BT curves of reference PES (grey), PES + NIP (blue) and PES + MIP-E2 (pink) composite membranes for filtration of E2 water solution in three cycles.

potential adsorption capability is exhibited up until their own saturation point is achieved, whereas the reference PES show indications of saturation near the end of the cycles. The steadily declining curve for E2 concentration in the permeates in every next cycle could be due to the additional regeneration step that may cause polymer swelling, making the adsorber particles more exposed and their pores enlarged. In the later cycles, the PES + MIP-E2 composite membrane exhibits slightly higher performance than the PES + NIP membrane. Since both particle types experience polymer swelling, the pore expansion in MIPs exposes more specific binding sites, leading to higher adsorption capacity. In contrast, NIPs rely on non-specific binding, resulting in surface saturation and allowing E2 concentrations in the permeate to rise in the later cycles. Through this clarification, supported by the BT curves and adsorption loading results, the composite membranes containing MIPs indicate higher adsorption capacity in later cycles than reference PES and composite membranes with NIPs.

TST adsorption loading. Fig. 6 displays the adsorption loading results for TST for the three membrane systems---PES, PES + NIP, and PES + MIP—across three adsorption cycles. The average results are comprised of three consecutive measurements. Following the filtration of 50 mL of 5 mg L^{-1} TST solution through the reference PES system, the amount of TST adsorbed relative to the total weight of the system reaches 0.15 ± 0.12 μg mg^{-1} in the first cycle. In contrast to the E2 adsorption loading on the reference PES, the TST adsorption loadings for the second and third cycles exhibit similar values, suggesting that the regeneration step has no effect on the TST adsorption. Furthermore, TST exhibits a lower adsorption affinity towards PES when compared to E2, with E2 being approximately five times more adsorptive on the PES membrane surface than TST. The TST adsorption loading values increase from 0.26 ± 0.21 μg mg^{-1} in the first cycle to 0.41 ± 0.18 μg mg^{-1} in the third cycle over the adsorption cycles

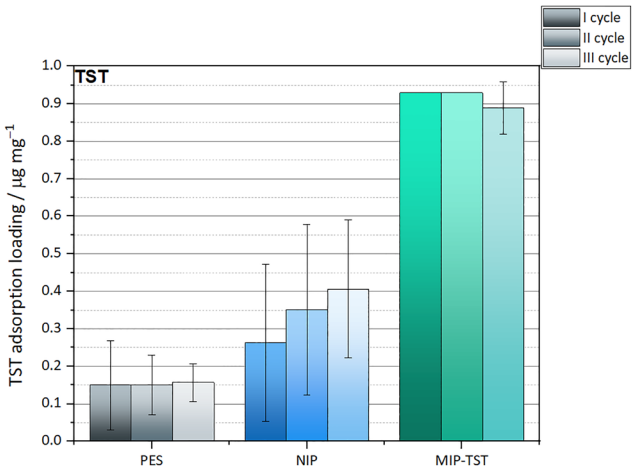

Fig. 6 TST adsorption loading (µg mg^{-1}) on reference PES, PES + NIP and PES + MIP-TST in three adsorption cycles.

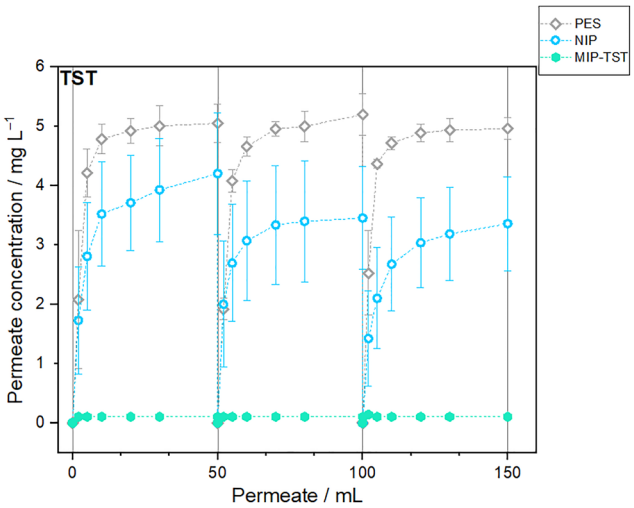

Fig. 7 BT curves of reference PES (grey), PES + NIP (blue) and PES + MIP-TST (green) composite membranes for filtration of TST water solution in three cycles.

with the PES + NIP composite membrane. With the addition of NIP particles, the TST adsorption loadings increase with each succeeding cycle (Fig. 6), opposed to the TST adsorption on reference PES. This implies that the pores of NIP particles swell due to EtOH washing, increasing their surface area and, consequently, their adsorption capacity. A high average adsorption loading of 0.93 µg mg^{-1} was recorded in the first and second cycles of TST adsorption loading on the PES + MIP-TST composite membrane. The measurement of the identical quantity of residing TST concentrations in the filtrate at the end of the dynamic adsorption experiments for all three measurements resulted in the same value for the first two cycles, due to the remaining TST concentrations in the filtrate being below the detection threshold of the instrument (<0.1 mg L^{-1}). As a result, error bars are too small to be visible in Fig. 6 for these values. An adsorption loading of 0.89 $\pm$ 0.07 µg mg^{-1} was recorded in the last cycle, demonstrating that the TST adsorption loading continues to be higher than it is with the reference PES and PES + NIP composite membranes, even after two regeneration steps.

Similarly to the BT curves for E2, Fig. 7 displays the BT curves for TST throughout the duration of three adsorption cycles with a comparable pattern for the TST concentration (mg L^{-1}) in the permeate. Over the course of one filtration cycle, the TST concentration gradually increases until it reaches a saturation plateau, which prevents further TST adsorption. For the reference PES membrane system, this pattern is evident throughout the three cycles of dynamic TST adsorption experiments. With the use of the PES + NIP composite membranes, the TST adsorption tests for each cycle reveal lower levels of TST present in the permeate than the reference PES. Furthermore, the PES + NIP composite membrane exhibits improved TST adsorption capacity over cycles as well as regeneration with each additional cycle. The PES + MIP-TST composite membranes outperform this adsorption capability, with their BT curves showing a TST permeate concentration that is five times lower than that of the reference PES. Moreover, these BT curves show no inclination and stay constant over all cycles as the permeate concentration is below the detection limit of the instrument. The implemented regeneration processes between cycles are considered the reason for the absence of a breakthrough point. This performance of the PES + MIP-TST composite membranes indicates both their high degree of adsorption and stability throughout each cycle. Upon comparison between the NIP and MIP composite membranes, the reduced TST adsorption on the PES + NIP composite membranes is more evident than that observed for E2. Moreover, the PES + MIP-TST composite membranes exhibit a higher adsorption capacity than their E2 counterparts.

E2-TST adsorption loading. The adsorption loadings for E2 and TST over three adsorption cycles for three membrane systems: PES, PES + NIP, and PES + MIP are shown on Fig. 8. E2 and TST adsorption loadings for all membrane systems were assessed three times, with the average results depicted in Fig. 8a and b, respectively. The dynamic adsorption tests were conducted using an E2-TST mixture solution, consisting of 2.5 mg L^{-1} E2 and 2.5 mg L^{-1} TST, totaling 5 mg L^{-1} of EDC. 50 mL of this mixture was filtered through the reference PES membrane system, and an additional blank sample with 2.5 mg L^{-1} TST (without E2) was prepared and fluorescence measurements for E2 were recorded. Separately, absorbance values for TST were recorded. No interference at the detecting wavelength was confirmed by both measurements. The first cycle for the reference PES resulted in 0.24 $\pm$ 0.09 µg mg^{-1} of adsorbed E2. The values of the TST absorbance in the first cycle for this membrane system exhibited 0.09 $\pm$ 0.01 µg mg^{-1}. Following the first cycle, the influence of the additional washing procedures caused slightly increased E2 adsorption loading on PES during the second and third cycles, whereas the TST adsorption loading slightly decreased, confirming the lower adsorption affinity of TST towards PES than E2.

As observed in Fig. 8a, the PES + NIP composite membrane exhibits lower E2 adsorption loading for each of the three cycles

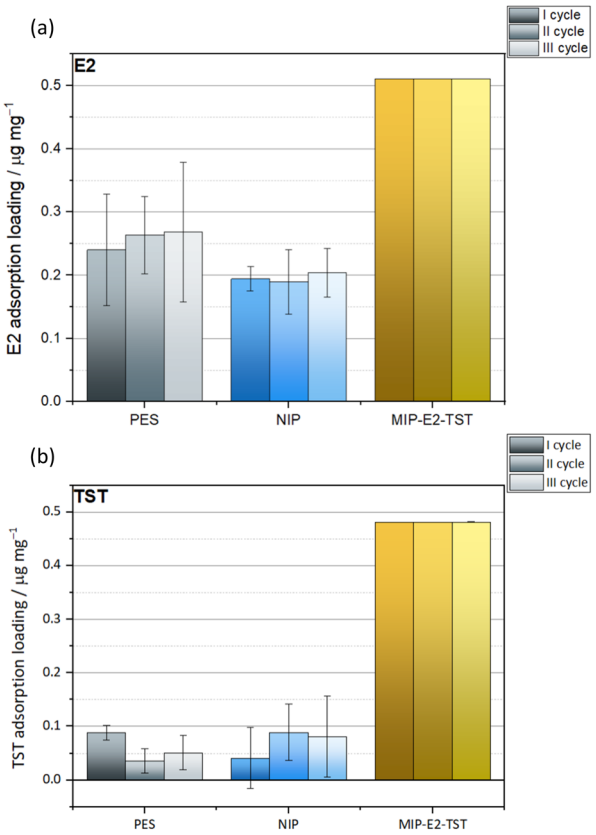

Fig. 8 Adsorption loading (μg mg^{-1}) of: (a) E2 and (b) TST on reference PES, PES + NIP and PES + MIP-E2-TST in three adsorption cycles.

when compared to the reference PES. This contrasts with the prior claim that the addition of NIP particles would result in more E2 adsorption. The presence of both E2 and TST in the filtered solution may be the cause of the decreased E2 adsorption in the PES + NIP composite membranes. As the NIPs are not molecularly imprinted, E2 and TST would have to compete for the same adsorption sites on the surface of the NIPs. As shown in Fig. 4, when E2 was the only EDC present, the PES + NIP composite membrane exhibited slightly higher E2 adsorption than the reference PES, leading to an overall comparable adsorption loadings between the two. Upon introducing the E2-TST mixture, the competing adsorption and varying adsorption affinities of the EDCs, causes E2 to adsorb less on PES + NIP than on the reference PES.

As previously seen, Fig. 6 illustrated how the addition of NIPs increased the TST adsorption loading, when compared to the reference PES. This points out that TST exhibits more adsorption on PES + NIP than only on PES. In the case when an E2-TST mixture is added to the reference PES (Fig. 8b), TST adsorption loadings are significantly lower than those of E2. This is also evident in the case of PES + NIP composite membrane, where TST adsorbs less on NIP surface than E2. The average E2 adsorption loading of the PES + NIP composite membrane is 0.19 ± 0.02 μg mg^{-1} for the first cycle, and by the third cycle, it has slightly increased to 0.20 ± 0.04 μg mg^{-1}, whereas the average TST adsorption loading for this system reached only 0.08 ± 0.07 μg mg^{-1} in the last cycle.

The double-target PES + MIP-E2-TST composite membrane, exhibited a high average E2 adsorption loading of 0.51 μg mg^{-1} after the filtration of E2-TST mixture across all three cycles. Each filtrate had the same amount of residual E2 concentrations, detected below the threshold of the instrument (<0.1 mg L^{-1}), resulting in the same adsorption loading values and error bars too small to be visible in Fig. 8a. Similarly, because of undetectable TST concentrations in the filtrate, TST adsorption loading was 0.48 μg mg^{-1} for all three cycles, with indistinguishable error bars (Fig. 8b). This further demonstrates more selectivity of the double-target MIPs toward both E2 and TST compared to NIPs. As these membranes are the prime focus in this research, it is important to note that the adsorption values correspond to the total mass of the sandwich system (100 mg MIPs and ≈150 mg of PES membranes). When normalized to the mass of active MIPs, the adsorption capacity increases from 0.5 to 1.25 μg mg^{-1} per analyte, corresponding to a total of 2.5 μg mg^{-1}. This highlights the dilution effect caused by the PES membranes, which may lead to underestimation, as adsorption capacities are often reported per gram of MIP only.[40,41] Moreover, since the values are given per target, the combined capacity (≈1 μg mg^{-1}, or 2.5 μg mg^{-1} based on MIP mass) is comparable with the amounts reported for the single-target systems described above.

The BT curves for E2 and TST across three adsorption cycles for the three membrane systems, reference PES, PES + NIP, and double-target PES + MIP-E2-TST composite membranes are shown in Fig. 9a and b, respectively. Fig. 9a shows the E2 concentration in the permeate progressively rising over the course of one filtration cycle, as previously observed. The reference PES membrane systems saturate in the second half of each cycle, preventing additional E2 adsorption. In comparison to the reference PES, the E2 concentration in the later cycles is slightly lower for the PES + NIP composite membranes. This was also observed on Fig. 5 when 5 mg L^{-1} E2 solution was filtered through a PES + NIP composite membrane. The inclination in the BT curve suggests that these membranes are nearing their saturation point. The PES + MIP-E2-TST composite membranes, in contrast, exhibit no BT points for E2 concentrations during any cycle, and the E2 concentration remains below the detection limit of the instrument (Fig. 9a). This behavior was not observed during the E2 adsorption tests using PES + MIP-E2 composite membranes, leading to the MIP-E2 particles being less specific towards E2 than the double-target MIPs made for both, E2 and TST. Two potential explanations to this behavior include the use of lower E2 concentration (2.5 mg L^{-1} as opposed to 5 mg L^{-1}) in the experiments and the possibility that double-target imprinting provides a greater variety of binding sites within the polymer matrix. Since E2 and TST share structural similarities, E2 molecules may bind to TST-imprinted cavities, thus resulting in a higher E2 adsorption. The binding cavities formed with the E2-TST template may accommodate a wider range of spatial orientations for E2 or TST molecule when reintroduced. It is expected that more molecules can potentially be adsorbed in the cavities, than

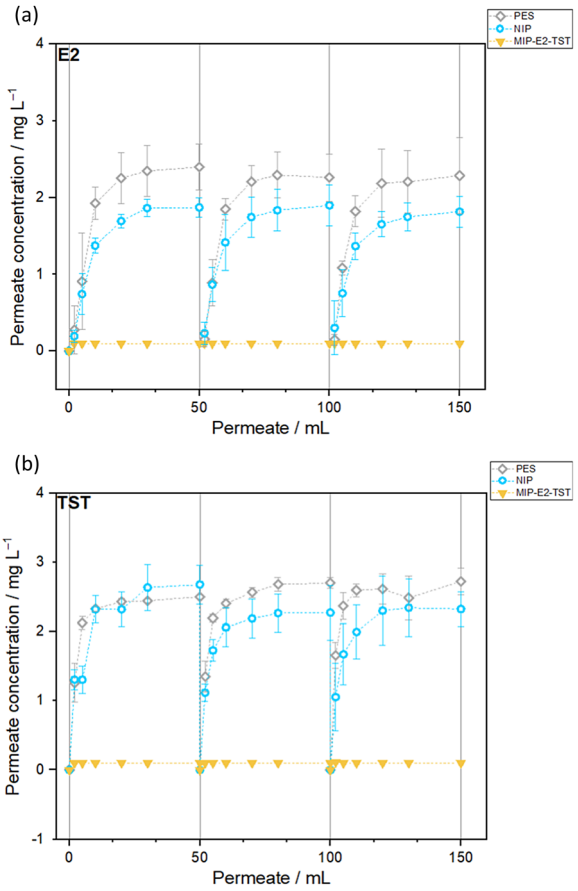

Fig. 9 BT curves of reference PES (grey), PES + NIP (blue) and PES + MIP-E2-TST (yellow) composite membranes for filtration of: (a) E2 and (b) TST water solution in three cycles.

when the particles are imprinted with a single EDC. Additionally, using two molecules as a template during the polymerization process, may increase the porosity and, therefore, surface area, which would contribute to an enhanced adsorption performance.[53,54]

Similar trends to the E2 BT curves are observed in Fig. 9b, which displays the BT curves for TST concentrations during three adsorption cycles. The gradual increase in TST concentration in the first cycle of the TST adsorption test for the reference PES reaches a saturation plateau that resembles the E2 BT curves. This is observed for the second and third cycles as well. The BT curve of the PES + NIP composite membrane in the first cycle is indistinguishable from that of the reference PES, confirming that both membrane systems exhibit similarly reduced TST adsorption when the E2-TST mixture is introduced. The later cycles show a similar pattern, indicating that the regeneration steps do not influence TST adsorption. This can be attributed to the stronger non-specific binding of E2 onto NIPs compared to TST. Therefore, E2 must be the primary factor for this pattern, as TST alone shows slightly higher adsorption on NIPs than on PES (Fig. 6). However, as with the BT curves for the same membrane systems in Fig. 9a, the BT points for TST concentrations in the PES + MIP-E2-TST composite membranes are absent throughout all cycles, and the TST concentration remains below the detection limit of the instrument. Moreover, there are no breakthrough points due to the regeneration processes in between cycles. This behavior of PES + MIP-E2-TST composite membranes shows their stability and high adsorption capacity across all cycles demonstrating the improved efficacy of composite membranes containing MIPs. With the introduction of double-target MIPs, the adsorption capacity as well as the reusability of the membranes are further increased for both EDCs.

Selectivity

TST tests with MIP-E2. To evaluate the selectivity of the MIPs, dynamic adsorption experiments were conducted using TST with the PES + MIP-E2 membrane system and E2 with the PES + MIP-TST system. Fig. 10a shows the TST adsorption loadings for the three membrane systems: PES, PES + NIP, and PES + MIP-E2 in three adsorption cycles. The TST adsorption loading section covered the findings for the first two membrane systems. The adsorption loading of TST in the first cycle for PES + MIP-E2 was 0.65 ± 0.16 μg mg^{-1}, which slightly increased during the third cycle to 0.70 ± 0.16 μg mg^{-1} through

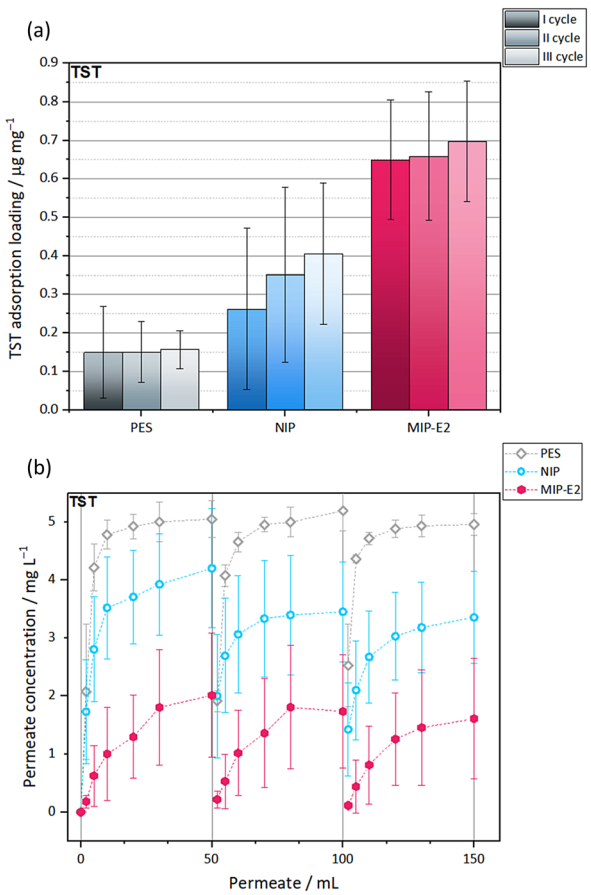

Fig. 10 (a) TST adsorption loading (μg mg^{-1}) on reference PES, PES + NIP and PES + MIP-E2 in three adsorption cycles; (b) BT curves of reference PES (grey), PES + NIP (blue) and PES + MIP-E2 (pink) composite membranes for filtration of TST water solution in three cycles.

regeneration. This indicates that the E2-imprinted MIP exhibits lower selectivity toward TST compared to E2, as reflected by the E2 adsorption loading of 0.82 ± 0.12 μg mg^{-1} observed in the third cycle. Fig. 10b displays the BT curves for the measured TST during three adsorption cycles. The permeate TST concentration for the reference PES and PES + NIP membrane systems exhibits the previously mentioned patterns. The PES + MIP-E2 composite membrane displays the increase in TST concentration gradually and approaches a moderate saturation in the third cycle. In contrast to the E2 testing with this composite membrane, the permeate E2 concentration was lower than the TST concentration. This implies that the PES + MIP-E2 composite membrane is more selective towards E2 than TST, even though, similarly to the other membrane systems, TST adsorption continues onto the E2-imprinted composite membrane during each cycle until saturation is reached.

E2 tests with MIP-TST. The E2 adsorption loadings for the three membrane systems: PES, PES + NIP, and PES + MIP-TST in three adsorption cycles are exhibited on Fig. 11a. The results for the first two membrane systems were discussed in the E2 adsorption loading section. With E2 filtration through PES + MIP-TST, E2 exhibited adsorption loading of 1.05 ± 0.02 μg mg^{-1} which remained throughout the cycles at a similar value. This shows an increased selectivity of the TST-imprinted MIP towards E2 than TST throughout the cycles, as reflected by the TST adsorption loading of 0.89 ± 0.07 μg mg^{-1} observed in the third cycle (Fig. 6). To explain the higher E2 adsorption on TST-imprinted particles, Table 1 provides the topological polar surface area (TPSA) values of the investigated EDCs. TPSA, expressed in $Å^2$, estimates the polar surface area of a molecule based as the summed surface contributions of its polar atoms.[51] Among the compounds examined, TST has the lowest TPSA of 37.3 $Å^2$, whereas E2 exhibits a higher value of 40.5 $Å^2$. The cavities formed using TST as the template can accommodate the more polar E2 molecules, even though TST is the less polar molecule, likely due to the greater availability of functional groups from the functional monomer (MAA) within those cavities, needed to stabilize the TST-monomer interactions. After removing the template and reintroducing TST, it interacts strongly with the binding site through hydrogen bonding facilitated by its single hydroxyl group as well as hydrophobic interactions. Moreover, the binding cavities result in being more polar than the TST molecule itself, due to the cluster of functional groups from MAA. When an E2 molecule is introduced, it would also bind to these cavities. E2 contains two hydroxyl groups (with one of them phenolic), through which it forms twice as many hydrogen bonds with MAA than TST (Fig. 1). The phenolic hydroxyl group is more acidic, making it a stronger hydrogen-bond donor, and the aromatic ring in E2 enables additional π interactions. These factors provide E2 with more interaction sites per molecule, contributing to its enhanced affinity for the TST-imprinted cavities.

Fig. 11b shows the BT curves for E2 during three adsorption cycles. The permeate E2 concentrations for the reference PES and PES + NIP membranes follow the previously described trends. In contrast, the PES + MIP-TST composite membrane exhibits a much lower E2 concentration, which increases slightly toward the end of each cycle. In contrast to the TST tests, where the permeate TST concentration remained below the detection limit of the instrument yielding no BT points, the E2 filtration showed an increase in E2 concentration towards the end of each cycle as expected, indicating that despite substantial E2 adsorption (Fig. 11a), the presence of BT points during E2 testing suggests that the TST-imprinted composite membrane exhibits preferential selectivity toward TST over E2.

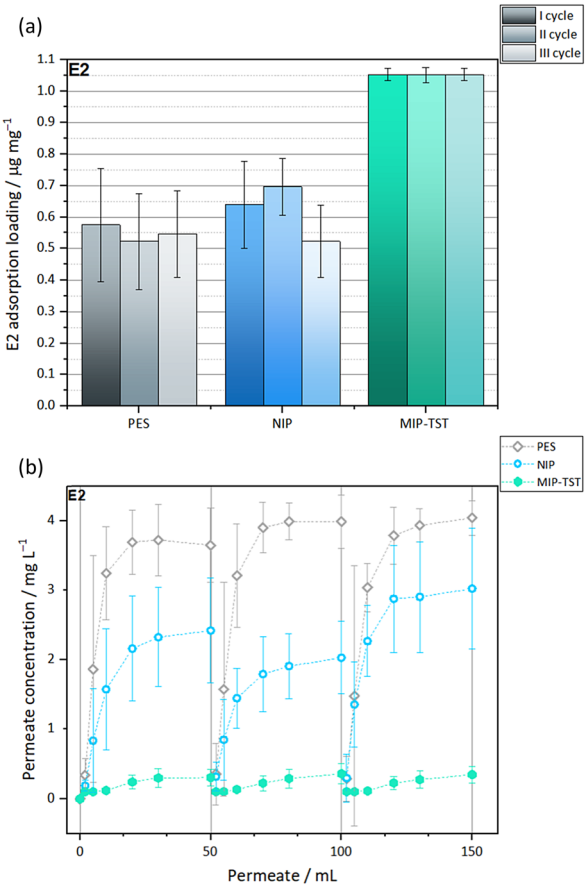

Fig. 11 (a) E2 adsorption loading (μg mg^{-1}) on reference PES, PES + NIP and PES + MIP-TST in three adsorption cycles; (b) BT curves of reference PES (grey), PES + NIP (blue) and PES + MIP-TST (green) composite membranes for filtration of E2 water solution in three cycles.

Returning to the double-target MIP composite membranes, this behavior was not observed: when filtering either E2 or TST, no EDCs were detected in the filtrate. This clearly indicates that using a 1 : 1 mixture of E2 and TST as templates creates distinct binding cavities for both analytes, offering more effective and sustained adsorption than single-template MIPs or NIPs.

BPA adsorption loading. To evaluate the selectivity of the E2- and TST-imprinted particles towards these EDCs, dynamic adsorption experiments were conducted using BPA, another EDC that, unlike E2 and TST, does not contain a steroid structure. The adsorption loadings for the four membrane systems: PES, PES + NIP, PES + MIP-E2, and PES + MIP-TST in three adsorption cycles are exhibited on Fig. 12. In the first membrane system, BPA exhibited adsorption loading of 0.35 ± 0.02 μg mg^{-1} during the

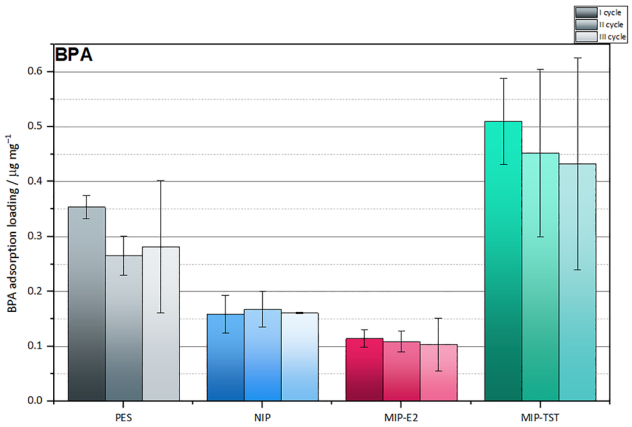

Fig. 12 BPA adsorption loading (μg mg^{-1}) on reference PES, PES + NIP, PES + MIP-E2 and PES + MIP-TST in three adsorption cycles.

first cycle with no subsequent increase upon regeneration. Moreover, this step showed negligible changes between cycles upon filtering 5 mg L^{-1} BPA solution through PES + NIP composite membrane, as the adsorption loading 0.16 ± 0.03 μg mg^{-1} for the first cycle remained similar throughout the rest of the cycles. The adsorption loadings for BPA for the third membrane system, PES + MIP-E2, followed a comparable trend as the previous system, displaying a BPA adsorption of 0.11 ± 0.02 μg mg^{-1} for the first cycle. In contrast to the higher E2 adsorption observed for the PES + MIP-E2 than PES + NIP, BPA showed lower adsorption on PES + MIP-E2 than the first two non-imprinted membrane systems. This indicates that the E2-molecular imprinting causes the particles to adsorb almost ten times more E2 than BPA. Nonetheless, this is not the case with the BPA adsorption loading for the PES + MIP-TST membrane system, where this composite membrane exhibits the highest BPA adsorption loading 0.51 ± 0.08 μg mg^{-1} measured in the first cycle. Although the adsorption decreased slightly in subsequent cycles, it remained the highest overall. This value corresponds to roughly half of the TST adsorption achieved by the same membrane in the first cycle (0.93 μg mg^{-1}). Furthermore, this behavior of the PES + MIP-TST composite membrane is similar to the E2 selectivity tests and could be attributed to the greater polarizability of BPA than E2, due to it containing two phenolic groups, meaning BPA could interact with the TST-imprinted cavities through hydrogen bonding, π interactions, and hydrophobic effects. Although BPA and E2 share the same TPSA value (40.5 $Å^2$), BPA is less effectively adsorbed than E2, primarily because BPA lacks a steroidal structure, limiting its geometric compatibility with the TST-imprinted cavities.

The BT curves for the tested BPA across three adsorption cycles are presented in Fig. 13. On Fig. 13a, the permeate BPA concentration (mg L^{-1}) follows a similar trend for the reference PES, PES + NIP and PES + MIP-E2 membrane systems. In each case, the gradual rise in BPA concentration during one filtration cycle reaches a saturation plateau, preventing further BPA adsorption. This behavior can be observed across all three cycles for the reference PES and PES + NIP composite membranes, suggesting that regeneration does not enhance BPA adsorption in subsequent cycles. The PES + MIP-E2 composite membranes display similar adsorption performance, with BT curves mirroring those of the non-imprinted membrane systems. Analogously, Fig. 13b shows the same trends for BPA for the first two membrane systems, but the BT curves for BPA for the PES + MIP-TST composite membrane exhibit a slower and more gradual increase in permeate BPA concentration before reaching the saturation plateau. This suggests continued BPA adsorption on this composite membrane throughout each cycle, until saturation is achieved, similar to the other membrane systems.

Relative adsorption percentages. The relative adsorption of each EDC (%) for the two membrane systems: PES + MIP-E2 and PES + MIP-TST are shown on Fig. 14a and b, respectively, as a summary of the results in this section. Fig. 14a exhibits the adsorption loadings of each EDC during the first cycle of a dynamic adsorption experiment with the PES + MIP-E2 membrane system. From these values, the adsorption of each EDC was expressed relative to the E2 loading, which was set to 100%. As shown in the previous detailed results, both TST and BPA show lower adsorption than E2, exhibiting 89% and 15%, respectively. Similarly, these relative percentages were calculated

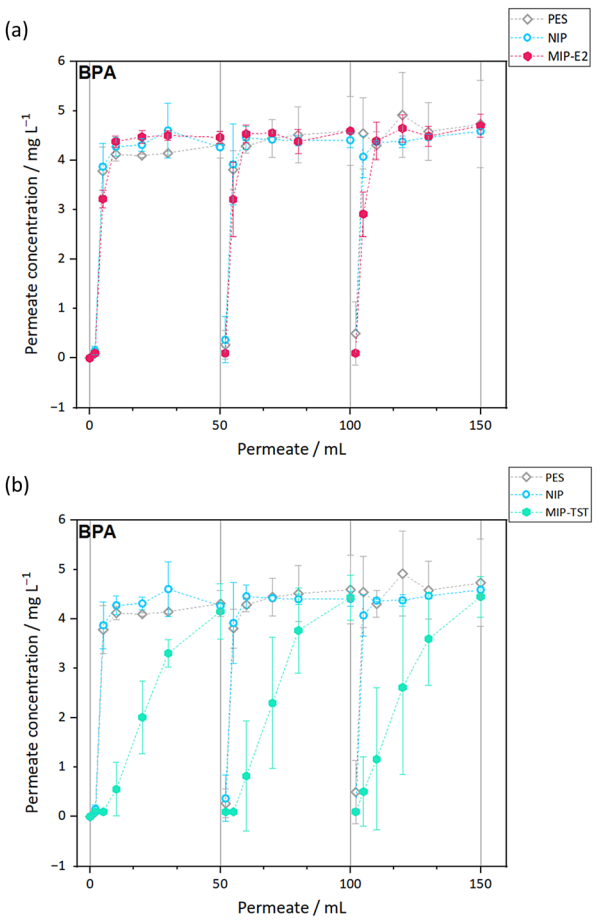

Fig. 13 BT curves of reference PES (grey), PES + NIP (blue) and composite membranes: (a) PES + MIP-E2 (pink) and (b) PES + MIP-TST (green) for filtration of BPA water solution in three cycles.

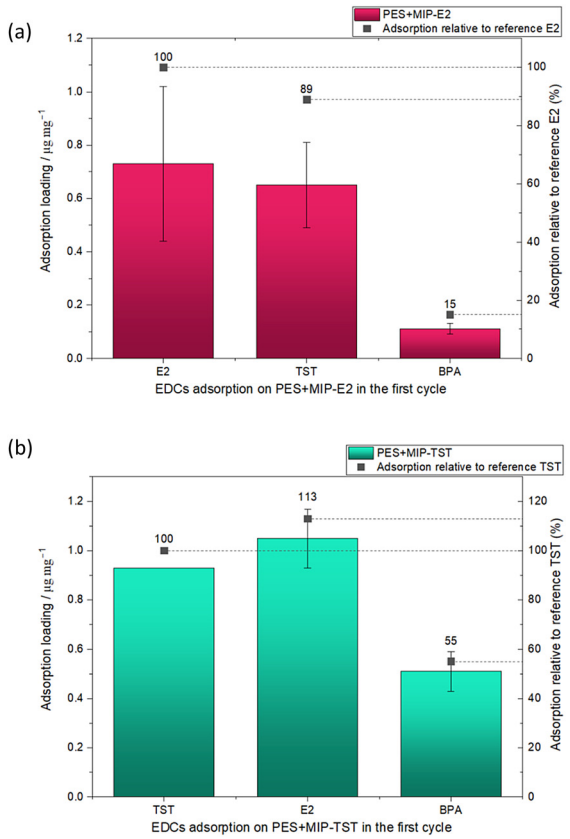

Fig. 14 Summarized overview of the EDC adsorption of E2, TST and BPA on: (a) PES + MIP-E2 (pink) and (b) PES + MIP-TST (green) in the first cycle of a dynamic adsorption test.

for PES + MIP-TST (Fig. 14b), where TST adsorption was scaled to 100%. E2 adsorption reached 113%, exhibiting higher E2 uptake on this membrane system than TST as previously discussed. BPA adsorption also reached 55% relative to TST, once again showing that PES + MIP-TST exhibits higher adsorption capacity than PES + MIP-E2, even for BPA.

Conclusions

In this study, composite MF membranes were developed and evaluated for the selective removal of EDCs, specifically E2 and TST. The membranes combined PES with MIP particles synthesized *via* precipitation polymerization in the presence of E2 and TST to create specific recognition sites (double-target imprinted), while NIPs served as references. Subsequently, sandwich-type composite membranes were prepared by embedding MIP/NIP particles between two PES layers, which were characterized using SEM, water permeance, and adsorption tests. Adsorption experiments confirmed that E2- and TST-imprinted membranes exhibited high adsorption capacities when compared to NIP or PES membranes. The double-target MIP membranes effectively adsorbed both E2 (0.51 μg mg^{-1}) and TST (0.48 μg mg^{-1}), confirming successful dual adsorption and enhanced binding site density. Selectivity testing revealed that TST-imprinted particles showed characteristics of a multi-adsorptive surface, capable of binding not only TST but also E2 and BPA, whereas E2-imprinted particles did not exhibit this broader adsorption capability. Reusability tests showed improved adsorption over cycles due to polymer swelling and pore expansion. Future work should focus on reducing particle agglomeration, enabling their full incorporation into the MF membrane scaffold through alternative methods (*e.g.*, *via* NIPS or EB irradiation), scaling up production, and testing in real water matrices.

Author contributions

Jane Neshovski: data curation, investigation, methodology, validation, visualization, writing – original draft, writing – review and editing. Daniel Breite: conceptualization, project administration, supervision, writing – review and editing. Zahra Niavarani: conceptualization, methodology, supervision. Andrea Prager: investigation. Dirk Enke: supervision, writing – review and editing. Agnes Schulze: project administration, resources, supervision, writing – review and editing.

Conflicts of interest

There are no conflicts to declare.

Data availability

The data supporting this article have been included as part of the Supplementary information (SI). Supplementary information: SEM pictures, optical microscopy pictures, and Tables S1–S4. See DOI: https://doi.org/10.1039/d6ma00574h.

Acknowledgements

The financial support by the Federal State of Germany and the Free State of Saxony is gratefully acknowledged. The authors would also like to thank Mathias Kühnert, who provided the optical microscopy images in the supplementary material.

Notes and references

1 H. Kuhl, Pharmacology of estrogens and progestogens: influence of different routes of administration, *Climacteric*, 2005, **8**, 3–63.
2 A. D. Mooradian, J. E. Morley and S. G. Korenman, Biological Actions of Androgens, *Endocr. Rev.*, 1987, **8**, 1–28.
3 B. Yilmaz, H. Terekeci, S. Sandal and F. Kelestimur, Endocrine disrupting chemicals: exposure, effects on human health, mechanism of action, models for testing and strategies for prevention, *Rev. Endocr. Metab. Disord.*, 2020, **21**, 127–147.
4 M. F. M. A. Zamri, R. Bahru, F. Suja, A. H. Shamsuddin, S. K. Pramanik and I. M. R. Fattah, Treatment strategies for enhancing the removal of endocrine-disrupting chemicals in water and wastewater systems, *J. Water Process. Eng.*, 2021, **7**, 102017.

5 P. Rajasulochana and V. Preethy, Comparison on efficiency of various techniques in treatment of waste and sewage water – A comprehensive review, *Resour.-Effic. Technol.*, 2016, **2**, 175–184.
6 Y. Zhang and J. L. Zhou, Removal of estrone and 17β-estradiol from water by adsorption, *Water Res.*, 2005, **39**, 3991–4003.
7 F. Cecen and Ö. Aktaş, *Activated Carbon for Water and Wastewater Treatment*, John Wiley & Sons, Washington, DC, 2011.
8 C. Trellu, N. Oturan, F. K. Keita, C. Fourdrin, Y. Pechaud and M. A. Oturan, Regeneration of Activated Carbon Fiber by the Electro-Fenton Process, *Environ. Sci. Technol.*, 2018, **52**, 7450–7457.
9 A. F. S. Foureaux, E. O. Reis, Y. Lebron, V. Moreira, L. V. Santos, M. S. Amaral and L. C. Lange, Rejection of pharmaceutical compounds from surface water by nanofiltration and reverse osmosis, *Sep. Purif. Technol.*, 2019, **212**, 171–179.
10 J. Radjenović, M. Petrović, F. Ventura and D. Barceló, Rejection of pharmaceuticals in nanofiltration and reverse osmosis membrane drinking water treatment, *Water Res.*, 2008, **42**, 3601–3610.
11 M. Hafiz, A. H. Hawari, R. Alfahel, M. K. Hassan and A. Altaee, Comparison of Nanofiltration with Reverse Osmosis in Reclaiming Tertiary Treated Municipal Wastewater for Irrigation Purposes, *Membranes*, 2021, **11**, 32.
12 M. G. Shin, W. Choi, S. J. Park, S. Jeon, S. Hong and J. H. Lee, Critical review and comprehensive analysis of trace organic compound (TOrC) removal with polyamide RO/NF membranes: Mechanisms and materials, *Chem. Eng. J.*, 2002, **427**, 130957.
13 X. Jin, J. Hu and S. L. Ong, Influence of dissolved organic matter on estrone removal by NF membranes and the role of their structures, *Water Res.*, 2007, **41**, 3077–3088.
14 Z. Niavarani, D. Breite, A. Prager, B. Abel and A. Schulze, Estradiol Removal by Adsorptive Coating of a Microfiltration Membrane, *Membranes*, 2021, **11**, 99.
15 S. Chang, T. D. Waite, A. I. Schäfer and A. G. Fane, Adsorption of the Endocrine-Active Compound Estrone on Microfiltration Hollow Fiber Membranes, *Environ. Sci. Technol.*, 2003, **37**, 3158–3163.
16 M. Zielińska, K. Bułkowska, A. Cydzik-Kwiatkowska, K. Bernat and I. Wojnowska-Baryła, Removal of bisphenol A (BPA) from biologically treated wastewater by microfiltration and nanofiltration, *Int. J. Environ. Sci. Technol.*, 2016, **13**, 2239–2248.
17 T. Wang, J. He, J. Lu, Y. Zhou, Z. Wang and Y. Zhou, Adsorptive removal of PPCPs from aqueous solution using carbon-based composites: A review, *Chin. Chem. Lett.*, 2022, **33**, 3585–3593.
18 P. Márquez, A. Benítez, A. F. Chica, M. A. Martín and A. Caballero, Evaluating the thermal regeneration process of massively generated granular activated carbons for their reuse in wastewater treatments plants, *J. Cleaner Prod.*, 2022, **366**, 132685.
19 L.-H. Jiang, Y.-G. Liu, G.-M. Zeng, F.-Y. Xiao, X.-J. Hu, X. Hu, H. Wang, T.-T. Li, L. Zhou and X.-F. Tan, Removal of 17β-estradiol by few-layered graphene oxide nanosheets from aqueous solutions: External influence and adsorption mechanism, *Chem. Eng. J.*, 2016, **284**, 93–102.
20 F. G. Tamayo, E. Turiel and A. Martín-Esteban, Molecularly imprinted polymers for solid-phase extraction and solid-phase microextraction: Recent developments and future trends, *J. Chromatogr. A*, 2007, **1152**, 32–40.
21 H. Dong, A.-J. Tong and L.-D. Li, Syntheses of steroid-based molecularly imprinted polymers and their molecular recognition study with spectrometric detection, *Spectrochim. Acta, Part A*, 2003, **59**, 279–284.
22 M. Boukadida, A. Anene, N. Jaoued-Grayaa, Y. Chevalier and S. Hbaieb, Choice of the functional monomer of molecularly imprinted polymers: Does it rely on strong acid-base or hydrogen bonding interactions?, *Colloid Interface Sci. Commun.*, 2022, **50**, 100669.
23 B. Sellergren, Polymer- and template-related factors influencing the efficiency in molecularly imprinted solid-phase extractions, *TrAC, Trends Anal. Chem.*, 1999, **18**, 164–174.
24 B. Sellergren, *Molecularly imprinted polymers: man-made mimics of antibodies and their application in analytical chemistry*, Elsevier, 2000.
25 T. Curk, J. Dobnikar and D. Frenkel, Rational design of molecularly imprinted polymers, *Soft Matter*, 2016, **12**, 35–44.
26 D. Hong, C. Wang, L. Gao and C. Nie, Fundamentals, Synthetic Strategies and Applications of Non-Covalently Imprinted Polymers, *Molecules*, 2024, **29**, 3555.
27 M. Okan, V. Sanko, E. Yıldırım, H. C. Tekin and H. Külah, MIP-on-the-flow: Molecularly imprinted polymers in microfluidic sensing systems, *TrAC, Trends Anal. Chem.*, 2026, **194**, 118511.
28 M. D. Celiz, D. S. Aga and L. A. Colón, Evaluation of a molecularly imprinted polymer for the isolation/enrichment of β-estradiol, *Microchem. J.*, 2009, **92**, 174–179.
29 E. Benito-Peña, F. Navarro-Villoslada, S. Carrasco, S. Jockusch, M. F. Ottaviani and M. C. Moreno-Bondi, Experimental Mixture Design as a Tool for the Synthesis of Antimicrobial Selective Molecularly Imprinted Monodisperse Microbeads, *ACS Appl. Mater. Interfaces*, 2015, **7**, 10966–10976.
30 V. J. B. Ruigrok, M. Levisson, M. H. M. Eppink, H. Smidt and J. Van Der Oost, Alternative affinity tools: more attractive than antibodies?, *Biochem. J.*, 2011, **436**, 1–13.
31 I. Bakas, N. Oujji, E. Moczko, G. Istamboulie, S. Piletsky, E. Piletska, I. Ichou, E. Addi and T. Noguer, Molecular imprinting solid phase extraction for selective detection of methidathion in olive oil, *Anal. Chim. Acta*, 2012, **739**, 99–105.
32 I. Chianella, A. Guerreiro, E. Moczko, J. S. Caygill, E. V. Piletska, I. M. P. De Vargas Sansalvador, M. J. Whitcombe and S. A. Piletsky, Direct Replacement of Antibodies with Molecularly Imprinted Polymer Nanoparticles in ELISA—Development of a Novel Assay for Vancomycin, *Anal. Chem.*, 2013, **85**, 8462–8472.

33 E. Guihen, Nanoparticles in modern separation science, *TrAC, Trends Anal. Chem.*, 2013, **46**, 1–14.
34 E. Moczko, A. Guerreiro, E. Piletska and S. Piletsky, PEG-Stabilized Core–Shell Surface-Imprinted Nanoparticles, *Langmuir*, 2013, **29**, 9891–9897.
35 E. Moczko, A. Poma, A. Guerreiro, I. P. De Vargas Sansalvador, S. Caygill, F. Canfarotta, M. J. Whitcombe and S. Piletsky, Surface-modified multifunctional MIP nanoparticles, *Nanoscale*, 2013, **5**, 3733–3741.
36 G. Wulff, Fourty years of molecular imprinting in synthetic polymers: origin, features and perspectives, *Microchim. Acta*, 2013, **180**, 1359–1370.
37 A. Poma, A. Guerreiro, S. Caygill, E. Moczko and S. Piletsky, Automatic reactor for solid-phase synthesis of molecularly imprinted polymeric nanoparticles (MIP NPs) in water, *RSC Adv.*, 2014, **4**, 4203–4206.
38 K. Smolinska-Kempisty, A. Guerreiro, F. Canfarotta, C. Cáceres, M. J. Whitcombe and S. Piletsky, A comparison of the performance of molecularly imprinted polymer nanoparticles for small molecule targets and antibodies in the ELISA format, *Sci. Rep.*, 2016, **6**, 37638–37645.
39 C. Cáceres, C. Bravo, B. Rivas, E. Moczko, P. Sáez, Y. Garcia and E. Pereira, Molecularly Imprinted Polymers for the Selective Extraction of Bisphenol A and Progesterone from Aqueous Media, *Polymers*, 2018, **10**, 679.
40 Z. Zhongbo and J. Hu, Selective removal of estrogenic compounds by molecular imprinted polymer (MIP), *Water Res.*, 2008, **42**, 4101–4108.
41 Z. Niavarani, D. Breite, A. Prager, I. Thomas, M. Kuehnert, A. Bernd, R. Gläser and A. Schulze, Synthesis of composite imprinted polymer membranes for the selective removal of 17β-estradiol from water, *Mater. Chem. Front.*, 2023, **7**, 4460–4472.
42 L. P. dos Santos Xavier, A. C. Dias, B. E. L. Baeta, L. de Azevedo Santos, T. C. Ramalho, S. F. de Aquino and A. C. da Silva, Experimental and theoretical studies of solvent polarity influence on the preparation of molecularly imprinted polymers for the removal of estradiol from water, *New J. Chem.*, 2019, **43**, 1775–1784.
43 Y. Lin, Y. Shi, M. Jiang, Y. Jin, Y. Peng, B. Lu and K. Dai, Removal of phenolic estrogen pollutants from different sources of water using molecularly imprinted polymeric microspheres, *Environ. Pollut.*, 2008, **153**, 483–491.
44 K. Niedergall, M. Bach, T. Schiestel and G. E. M. Tovar, Nanostructured Composite Adsorber Membranes for the Reduction of Trace Substances in Water: The Example of Bisphenol A, *Ind. Eng. Chem. Res.*, 2013, **52**, 14011–14018.
45 Z. Liao, M. N. Nguyen, G. Wan, J. Xie, L. Ni, J. Qi, J. Li and A. I. Schäfer, Low pressure operated ultrafiltration membrane with integration of hollow mesoporous carbon nanospheres for effective removal of micropollutants, *J. Hazard. Mater.*, 2020, **397**, 122779.
46 J. K. Ali, M. A. Jaoude and E. Alhseinat, Polyimide ultrafiltration membrane embedded with reline-functionalized nanosilica for the remediation of pharmaceuticals in water, *Sep. Purif. Technol.*, 2021, **266**, 118585.
47 S. Uebele, T. Goetz, M. Ulbricht and T. Schiestel, Mixed-Matrix Membrane Adsorbers for the Simultaneous Removal of Different Pharmaceutical Micropollutants from Water, *ACS Appl. Polym. Mater.*, 2022, **4**, 1705–1716.
48 K. Niedergall, M. Bach, T. Hirth, G. E. M. Tovar and T. Schiestel, Removal of micropollutants from water by nanocomposite membrane adsorbers, *Sep. Purif. Technol.*, 2014, **131**, 60–68.
49 S. Balta, A. Sotto, P. Luis, L. Benea, B. Van der Bruggen and J. Kim, A new outlook on membrane enhancement with nanoparticles: The alternative of ZnO, *J. Membr. Sci.*, 2012, **389**, 155–161.
50 M. Lehmann, H. Brunner and G. E. M. Tovar, Selective separations and hydrodynamic studies: a new approach using molecularly imprinted nanosphere composite membranes, *Desalination*, 2002, **149**, 315–321.
51 P. Ertl, B. Rohde and P. Selzer, Fast Calculation of Molecular Polar Surface Area as a Sum of Fragment-Based Contributions and Its Application to the Prediction of Drug Transport Properties, *J. Med. Chem.*, 2000, **43**, 3714–3717.
52 Z. Niavarani, D. Breite, B. Ulutaş, A. Prager, Ö. Kantoğlu, B. Abel, R. Gläser and A. Schulze, Enhanced EDC removal from water through electron beam-mediated adsorber particle integration in microfiltration membranes, *RSC Adv.*, 2023, **13**, 32928–32938.
53 M. Tian, K. Yu, L. Li, Y. Wang, L. Guo, Z. Zhang, Y. Lu and L. Li, Fabrication of dual-template molecularly imprinted mesoporous silica for simultaneous rapid and efficient detection of bisphenol A and diethylstilbestrol in environmental water samples, *Anal. Methods*, 2019, **11**, 4761–4768.
54 W. Lu, J. Liu, J. Li, X. Wang, M. Lv, R. Cui and L. Chen, Dual-template molecularly imprinted polymers for dispersive solid-phase extraction of fluoroquinolones in water samples coupled with high performance liquid chromatography, *Analyst*, 2019, **144**, 1292–1302.